

# Estimation of state of charge integrating spatial and temporal characteristics with transfer learning optimization

September 2022

**Abstract.** State of charge (SOC) estimation of lithium-ion battery is of vital significance for the control strategy in the battery management system (BMS). To integrate the spatial and temporal characteristics of the data, and to accomplish the transfer of knowledge, a novel convolutional neural network-bidirectional long short-term memory network based on transfer learning optimization (CNN-BiLSTM-TF) is proposed to estimate SOC. In detail, the spatial and temporal features hidden in the data are learned through CNN and BiLSTM, respectively. Furthermore, the CNN-BiLSTM network is established under one working condition and transferred to other working conditions through transfer learning, from which the SOC can be estimated online. A lithium-ion battery dataset is applied to verify the proposed SOC estimation approach. The results of case study demonstrate that the estimation performance of CNN-BiLSTM-TF is better than some existing approaches.

## 1. Introduction

Lithium-ion batteries have wide applications in aerospace, vehicle engineering, energy storage system due to the advantages of stable electrochemical characteristics, high energy efficiency, long charge and discharge cycle [1, 2, 3]. State of charge (SOC) is a vital indicator to measure the health state of lithium-ion battery [4]. The United States Advanced Battery Consortium (USABC) defines SOC as the ratio between the present capacity ( $Q_p$ ) and the rated capacity ( $Q_r$ ) of the battery, which is shown in Eq. (1):

$$SOC = \frac{Q_p}{Q_r} \times 100\% \quad (1)$$

It should be noted that SOC is the basis of the charge and discharge control strategy for battery management system (BMS) of the electrical equipment, which ensures balanced operation of the battery [5]. Accurate estimation of SOC can enable the power performance of the battery to full play. Furthermore, the safety of the battery can be improved, and the overcharging and overdischarging can be prevented [6].

In the existing literature, the SOC estimation approaches can be roughly categorized by the model-based and the data-driven approaches. The model-based SOC estimation approaches analyze the operating mechanism using physical and chemical reaction theories. The equivalent circuit model (ECM) [7] and the electrochemical

model [8] are the two most commonly developed battery models in SOC estimation. Furthermore, in order to establish the mechanism model of the battery, the SOC estimation model can also be constructed through adaptive filtering algorithms such as Kalman filtering (KF) [9] and particle filtering (PF) [10]. Zhu et al. proposed a fuzzy KF based on RC equivalent circuit, which developed multiple linear regression to identify the model parameters [11]. Due to the complexity of the electrochemical reaction, the random dynamic load condition, and the uncertainty in the degradation process, there are still many difficulties in explaining the mechanism of the batteries. On this basis, there are notable limitation if the model-based approaches are used to estimate SOC.

Based on the characteristics of the current, voltage, temperature and other data collected during the operation of the lithium-ion battery, the data-driven approaches are developed by learning algorithms to achieve SOC estimation [12, 13, 14]. The advantage of the data driven-based approaches is that accurate mathematical model of the battery is not required, the SOC estimation can be accomplished only by the data picked up by sensors. Chao et al. proposed probability kernel regression algorithm on the basis of relevance vector machine (RVM) employing charged voltage and current to achieve online SOC estimation [14]. In order to promote estimation accuracy, Shen et al. proposed deep convolutional neural network (DCNN) with the advantages of local connectivity and shared weights to estimate SOC by employing data such as voltage, current and charging capacity in the charging process [15]. Considering time dependence in working process, Prakash et al. proposed an improved independent recurrent neural network (IndRNN) to estimate the SOC during random dynamic load charge and discharge process [16]. + (1) Zhang optimization parameters. (2) Fan: V-net (3) Yang: BiLSTM

In the existing literature, few have been reported applying hybrid neural networks based approaches. The study has shown that integrating multiple deep learning methods has ability to overcome the shortcomings of conventional network, thereby achieving better estimation performance [17]. Furthermore, few literature focus on the small sample problem. Considering this, the transfer learning has unique merits such as improving training efficiency, increasing data samples, which motivates this work to develop CNN-BiLSTM-TF based approach. + (4) Yang: v1 Zhang deep representation regularization

Considering the complexity of the electrochemical reaction and the influence of the load change, the diversification of the SOC exhibits strong nonlinearity and time-variation, which is difficult to obtain by direct measurement. In addition, the load conditions of batteries are random and dynamic, rather than charging and discharging by constant voltage or current under laboratory conditions, which adds difficulty to the SOC estimation [18]. Therefore, how to estimate SOC accurately under random dynamic load conditions needs further research.

Inspired by the data-driven approaches, this paper focuses on estimating SOC by convolution bidirectional long-short memory network based on transfer learning optimization (CNN-BiLSTM-TF). Multiple variables are acquired from working process as the features, which are used as the inputs of the neural network. Convolutional

- ① Since the load conditions of batteries are random and dynamic ...
- ② SOC estimation through hybrid neural network integrates multiple
- ③ To reasonably utilize the battery operational data under multiple

bidirectional long short-term memory (CNN-BiLSTM) network is constructed, and the estimation performance of the model is appraised by leave-one-out cross validation. Afterwards, CNN-BiLSTM network under one of the working conditions is transferred to other working conditions through model-based transfer learning (TF) to achieve parameter sharing, based on which the SOC can be estimated online. The main contributions of the proposed SOC estimation approach are summarized as follows:

- It is proposed to estimate SOC with the aid of convolutional neural network (CNN). The CNN can accomplish automatic weight-sharing and feature extraction of the historical data from battery operation through convolution and pooling operations at the spatial level, so as to obtain more abstract features.
- It is proposed to estimate SOC with the aid of bidirectional long short-term memory (BiLSTM) network. The forward and reverse time series data can be analysed at the temporal level, in order to extract time dependence feature. Moreover, effective feature extraction at spatial and temporal levels can be accomplished by integrating CNN and BiLSTM.
- Transfer learning is proposed to estimate SOC through the model-based approach to achieve parameter sharing, so that the CNN-BiLSTM network is optimized, which improves the SOC estimation performance.
- The proposed SOC estimation approach in this paper is verified by the battery dataset under random dynamic load condition provided by the NASA Ames Research Center. The results of case study demonstrate that the estimation performance of CNN-BiLSTM-TF is better than some existing approaches.

## 2. SOC estimation approach

### 2.1. Spatial feature learning

In order to learn the spatial feature of the data better, CNN is introduced in the approach. The advantages of CNN are that sparse interaction, weight sharing and automatic feature extraction can be accomplished through convolution kernel [19]. The spatial characteristics of the input data can be automatically extracted through convolution and pooling operation.

The essence of CNN is to extract spatial characteristics at various scales by establishing multiple convolution kernels, each of which is equal to a feature extractor. The convolution kernels slide in the input matrix, so that the weight information can be shared by the input matrix, which decreases the number of training parameters [20]. The convolution kernel is denoted as  $W = [w_{mn}]_{p \times q}$ , the input matrix is  $X = [x_{ij}]_{s \times t}$ , the output  $y$  at the coordinates  $(i, j)$  in the input matrix can be calculated as follow:

$$y = f \left( \sum_{m=1}^p \sum_{n=1}^q w_{mn} \cdot x_{i+m-1, j+n-1} + b \right) \quad (2)$$

where  $b$  is the offset vector,  $f$  is the activation function of the convolution kernel. In this paper, rectified linear unit (ReLU) is introduced as the activated function in this paper shown in Eq. (3):

$$f(x) = \max(x, 0) \quad (3)$$

With the superposition of convolutional layers, the dimension of the features will increase. Therefore, pooling operations are introduced to reduce dimensionality so that time-consuming and overfitting problems caused by high-dimensional data can be prevented [20].

## 2.2. Temporal feature learning

It cannot be ignored that the time dependence of the random charge and discharge process of the battery is of great significance. Traditional deep neural networks with memory capabilities, such as recurrent neural network (RNN) [21], are prone to problems including gradient disappearance and explosion when dealing with long time series. By contrast, long-short term memory (LSTM) network can effectively solve this problem. Considering above and the usage of information in the reverse time series data, this paper estimates the SOC with the aid of BiLSTM network.

The LSTM unit contains four parts, namely, input gate ( $i_t$ ), forget gate ( $f_t$ ), output gate ( $o_t$ ) and memory cell ( $c_t$ ). The input gate determines the information that needs to be input. The forget gate selectively forgets the secondary information. The output gate determines the proportion of the input information that can be used for the final output. The memory cell determines the memory of the LSTM unit at the previous moment. The unit output is the product of the value of the output gate and the value of the memory cell. The structure of LSTM unit is shown in Figure 1.

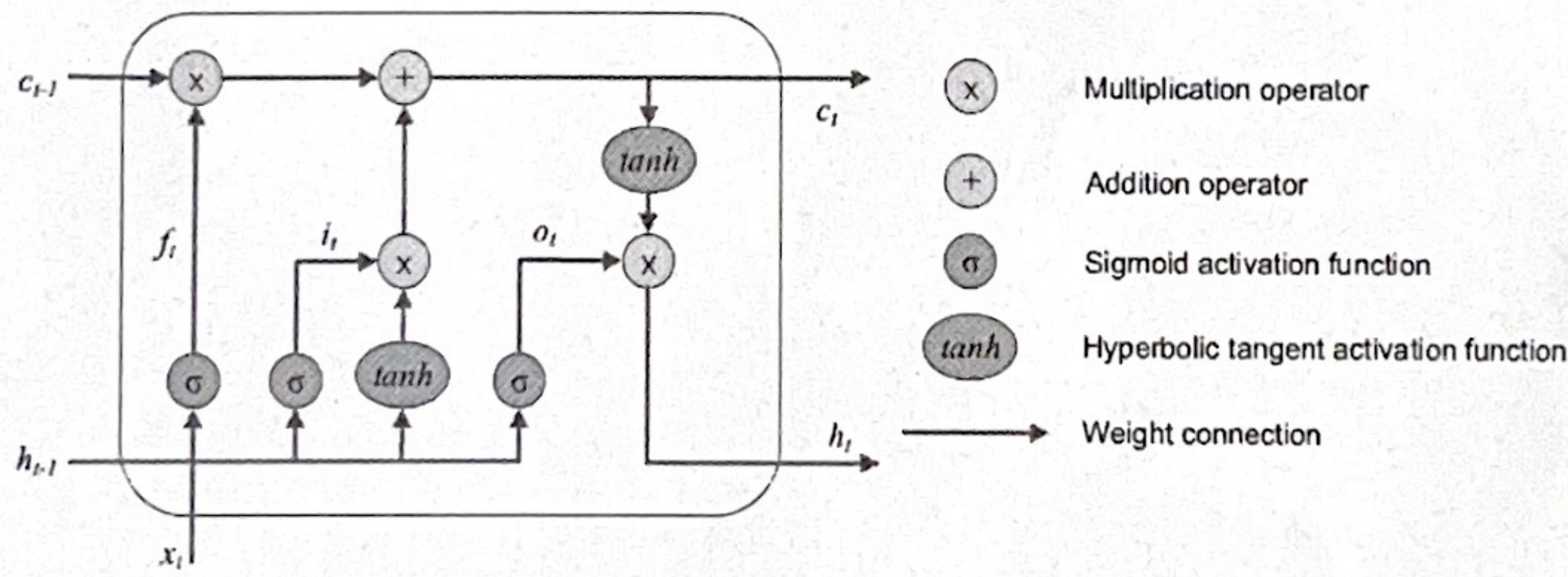


**Figure 1.** The structure of LSTM unit

The mathematical expressions of the internal structure are shown as Eqs. (4)–(8):

$$f_t = \sigma(W_f[x_t, h_{t-1}] + b_f) \quad (4)$$

$$i_t = \sigma(W_i[x_t, h_{t-1}] + b_i) \quad (5)$$

$$c_t = f_t * c_{t-1} + i_t * \tanh(W_c[x_t, h_{t-1}] + b_c) \quad (6)$$

$$o_t = \sigma(W_o[x_t, h_{t-1}] + b_o) \quad (7)$$

$$h_t = o_t * \tanh(c_t) \quad (8)$$

where  $x_t$  represents the input vector of the unit at time  $t$ ,  $h_{t-1}$  and  $h_t$  represent the state of the hidden layer at times  $t-1$  and  $t$ , respectively.  $f_t$ ,  $i_t$ ,  $o_t$ ,  $c_t$  denote the output of the forget gate, input gate, output gate, and memory cell.  $W_f$  and  $b_f$  represent the weight and offset vector of the forget gate, respectively.  $W_i$  and  $b_i$  represent the weight and offset vector of the input gate, respectively.  $W_c$  and  $b_c$  represent the weight and offset vector of the memory cell, respectively.  $\sigma$  and  $\tanh$  represent the sigmoid activation function and the hyperbolic tangent function, respectively.

The output of the LSTM unit is determined by the output of the gate structures, which can effectively avoid the gradient disappearance and explosion caused by weight multiplication. In order to use the past and future information, BiLSTM network is developed to use two different recurrent layers to obtain the hidden layer output from the forward and backward of the time series, which needs to be spliced. The structural of unfolding BiLSTM network in time is shown in Figure 2.

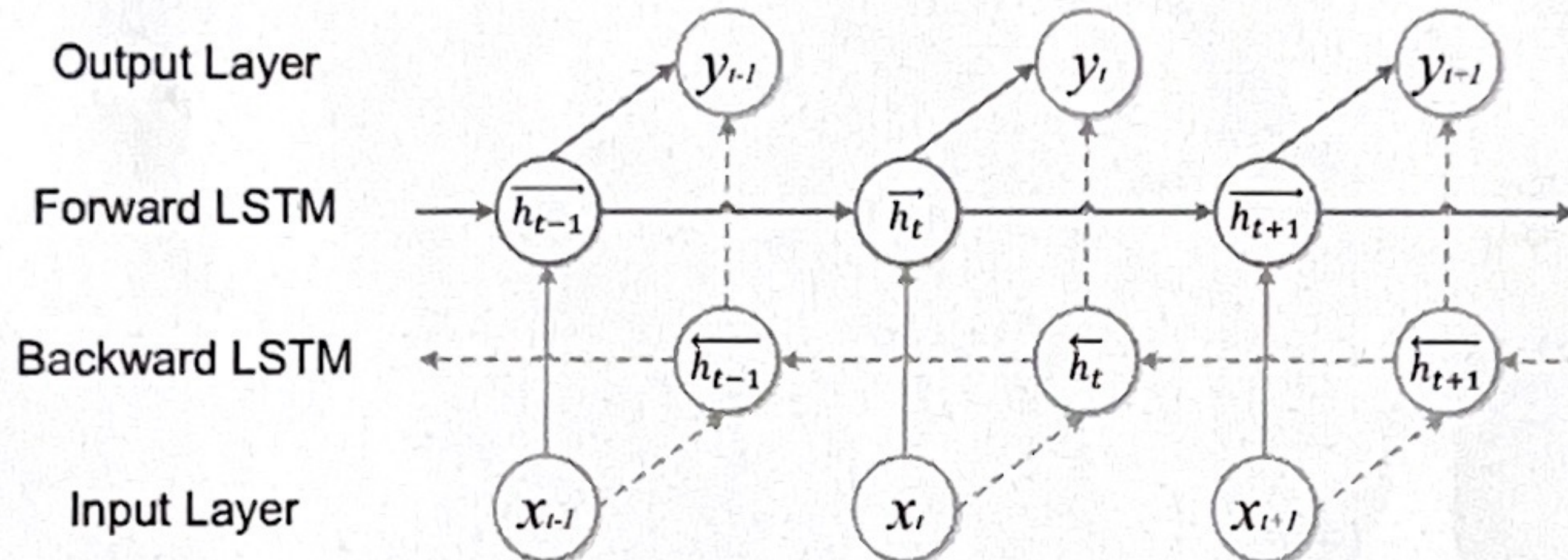


**Figure 2.** The structure of unfolding BiLSTM network

The forward and backward output sequence of the BiLSTM hidden layer at time  $t$  are shown as Eqs. (9)–(10):

$$\vec{h}_t = \overrightarrow{LSTM}(x_t, h_{t-1}, c_{t-1}) \quad (t \in [1, T]) \quad (9)$$

$$\overleftarrow{h}_t = \overleftarrow{LSTM}(x_t, h_{t-1}, c_{t-1}) \quad (t \in [T, 1]) \quad (10)$$

where the length of the input time series is  $T$ ,  $\overrightarrow{LSTM}$  and  $\overleftarrow{LSTM}$  represent the mapping relationship of the forward and reverse LSTM unit. The output of the hidden layer at the moment  $t$  is shown in Eq. (11):

$$h_t = [\vec{h}_t, \overleftarrow{h}_t] \quad (11)$$

Compared with basic LSTM, BiLSTM can use the past and future information to promote the estimation performance.

### 2.3. Transfer learning

Transfer learning is the learning process that the similarity between projects is employed to apply the knowledge gained in the old domain (source domain) to the new domain (target domain), the purpose of which is to pursue better results in new tasks. According to the different learning methods, transfer learning can be divided into four types which are based on samples, features, models and relationships [22]. The model-based transfer learning proposed in this paper achieves the migration by sharing the parameter information between the source domain and the target domain [23].

Considering that for the same type of lithium-ion battery in different working conditions, the working mechanism and internal characteristics are similar. Therefore, the model-based transfer learning can be developed to migrate the trained CNN-BiLSTM network under one working condition to other working conditions. In this sense, the similarity of battery under different working conditions is employed to achieve parameter sharing. The model-based transfer learning can enable the improvement of model training efficiency. Furthermore, the training samples can be increased to a certain extent, which alleviates the problem of limited fitting ability caused by small samples, so as to improve estimation performance. The formal expressions of the source domain  $D_S$  and target domain  $D_T$  of transfer learning of lithium-ion batteries are shown in Eqs. (12-13):

$$D_S = \{(x_i, y_i), (i = 1, 2, \dots, n), x_i \in R^l\} \quad (12)$$

$$D_T = \{(x_j, y_j), (j = 1, 2, \dots, m), x_j \in R^l\} \quad (13)$$

where  $x_i$  and  $y_i$  are the feature vector and label of the source domain, respectively.  $x_j$  and  $y_j$  are the feature vector and label of the target domain, respectively.  $i, j$  are the serial number of the source and target domain, respectively.  $n$  and  $m$  are the total number of samples in the  $D_S$  and  $D_T$ , respectively.  $l$  is the dimension of the feature vector.

In the proposed approach,  $D_S$  and  $D_T$  are the charge and discharge data of the battery under two random dynamic load conditions. The CNN-BiLSTM network is trained on the  $D_S$ . Furthermore, the trained neural network is transferred to the  $D_T$ . Specifically, the parameters of the spatial feature learning part CNN, are kept unchanged. Only the parameters of the temporal feature learning part BiLSTM, are update during the training process, thereby sharing the parameters. The knowledge of the  $D_S$  is transferred to the  $D_T$ , so that the training data are expanded invisibly without restarting the training of the network, which improves the training efficiency.

### 2.4. SOC estimation framework

The SOC estimation framework based on CNN-BiLSTM-TF proposed in this paper is shown in Figure 3. Multiple variables are acquired through the working process of the battery as the features. The battery dataset under one working condition is used as source domain to construct CNN-BiLSTM network. Afterwards, the battery datasets

**Algorithm 1: SOC estimation based on CNN-BiLSTM-TF**  
 Input : offline source data DS, target data DT, online target DT.  
 Output : Predicted battery's SOC in DT.

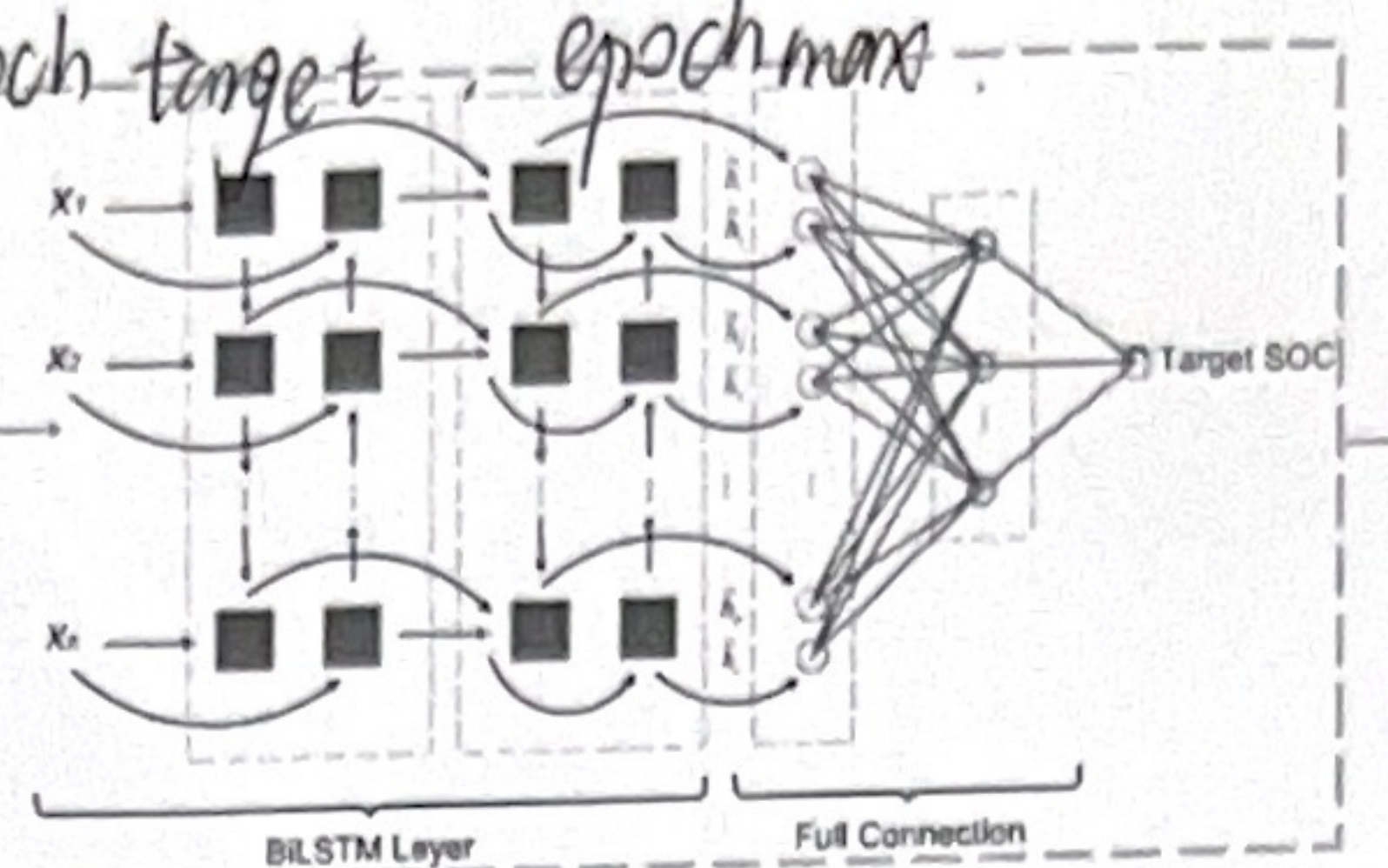
Step 0 Feature extraction for offline source domain data Eqs. (15)-118).

Preprint submitted to Measurement Science and Technology

② Initialize epoch<sub>source</sub> = epoch<sub>target</sub> = epoch<sub>max</sub>.

③ for epoch<sub>source</sub> < epoch<sub>target</sub>

④ Spatial feature learning (2) - (3).



⑤ Temporal feature learning (4)-(7)

⑥ Relationship between source features and SOC label.

⑦ Update Source network parameters

⑧ epoch<sub>source</sub> ++

⑨ end for

⑩ for epoch<sub>target</sub> < epoch<sub>max</sub>

⑪ trained neural network (source → target)

⑫ parameters of CNN-BiLSTM-TF

⑬ performance if BiLSTM is used under other working conditions are used as target domain. The corresponding feature extraction method is the same as the source domain. The trained CNN-BiLSTM network

⑭ Construct to achieve model parameter sharing. Finally, the CNN-BiLSTM-TF network can be applied for online SOC estimation, and the estimation performance is evaluated by the

⑮ Update target.

### 3. Case Study

#### 3.1. Data description

⑯ epoch<sub>target</sub> ++

⑰ end for

pseudo code of CNN-BiLSTM-TF  
 target features → SOC  
 (back-propagation).

To represent the effectiveness of the SOC estimation approach, the public dataset of battery charge and discharge process provided by the NASA is applied [24]. The dataset includes data such as current, voltage and temperature during charge and discharge of 28 batteries under seven working conditions. Each working condition includes the charge and discharge process of four 18650 lithium-ion batteries. These batteries in the dataset are working under random dynamic load conditions. In other words, the discharge current of the battery is random during operation. After a certain number of random charge and discharge cycles, the reference charge and discharge cycle is performed by the battery. In reference charge and discharge cycle, the battery is firstly charged at a

⑱ Online target domain prediction CNN-BiLSTM-TF.

⑲ Evaluate SOC estimation performances.

constant current of 2A until the voltage reaches 4.2V. Afterwards, the battery is switched to the constant voltage mode to continue charging. Finally, the battery is discharged at a constant current until the voltage reaches 3.2V [24]. On this basis, the current battery capacity is obtained by calculating the integral of current and time in the discharge process of the reference charge and discharge cycle, which provides a reference for SOC estimation. Table 1 represents the description of seven working conditions. The more details about batteries can be referred to the reference [24].

**Table 1.** Battery dataset description

| Condition | Battery Number | The description of charge and discharge situation   |
|-----------|----------------|---|
| 1         | 1,2,7,8        | Repeatedly charged to 4.2 V using a random time between 0.5h and 3 h, then discharged to 3.2 V using a random discharging current between 0.5A and 4A |
| 2         | 3,4,5,6        | Similar to Condition 1 except the charging cycle is regular   |
| 3         | 9,10,11,12     | Operated by using a random charging and discharging current between -4.5A and 4.5A  |
| 4         | 13,14,15,16    | Similar to Condition 1 except high-current discharge is likely to be used during the discharge process  |
| 5         | 17,18,19,20    | Similar to Condition 1 except low-current discharge is likely to be used during the discharge process   |
| 6         | 21,22,23,24    | Similar to Condition 5 except the ambient temperature is 40°C   |
| 7         | 25,26,27,28    | Similar to Condition 4 except the ambient temperature is 40°C   |

In the dataset, the batteries numbered 16 and 17 have missing data for a long time [25]. Therefore, the battery data under working conditions 4 and 5 are not employed for algorithm verification. In this sense, the battery data under working conditions 1, 2, 3, 6, and 7 are used to evaluate the proposed SOC estimation approach. The degraded curves of the battery capacity with time are shown in Figure 4.

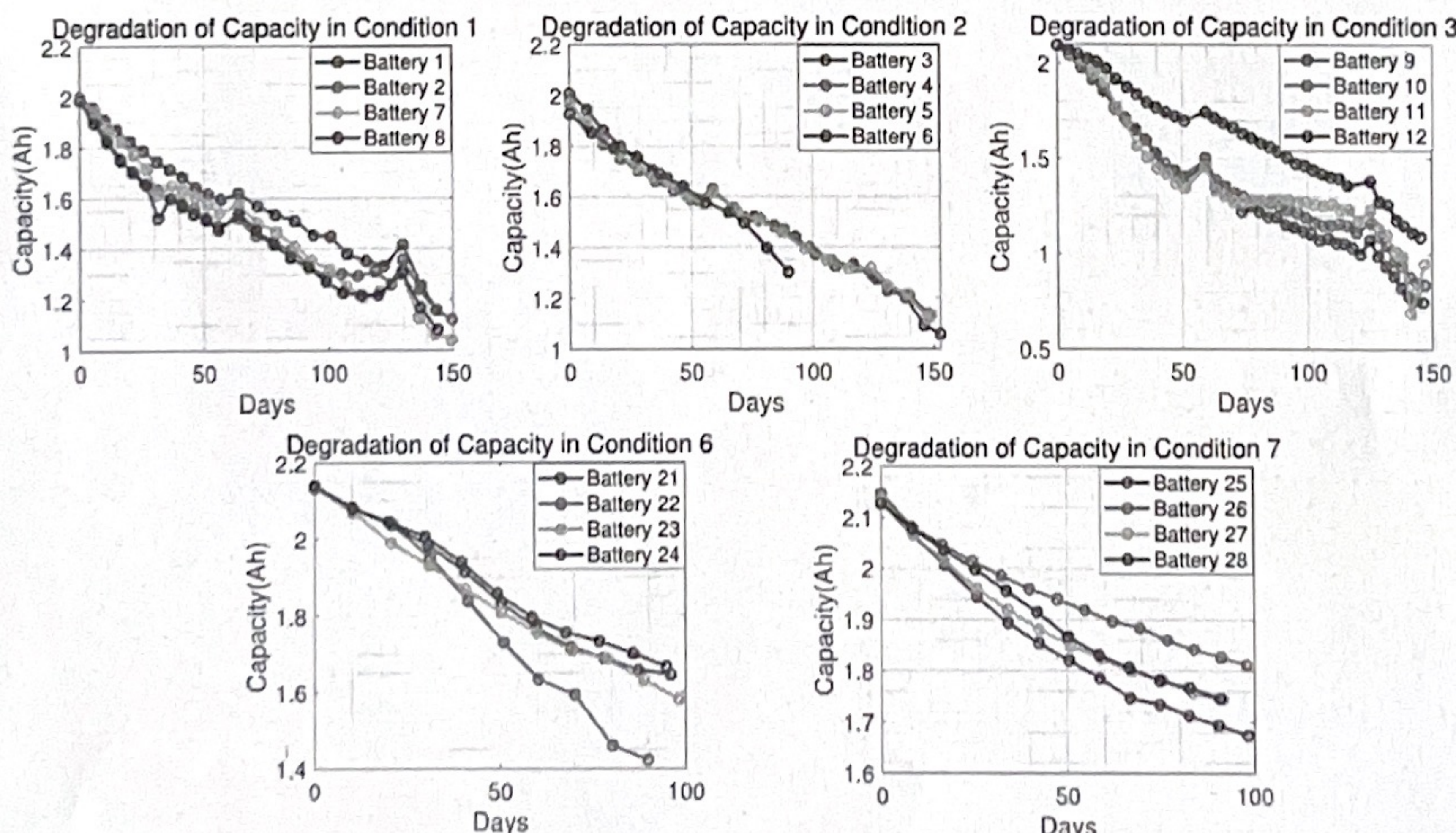


**Figure 4.** Degraded curves of the battery capacity with time under various conditions

### 3.2. Feature extraction

The battery dataset contains the current, voltage and temperature data of the battery under random dynamic load conditions. After a certain number of random charging and discharging processes, the reference charge and discharge cycle is performed, from which the present SOC of the battery is shown in Eq. (14):

$$SOC = \frac{\int_0^{t_d} i_d(\tau) d\tau}{Q_r} \quad (14)$$

where  $t_d$  is the time of the reference discharge process,  $i_d$  is the current during the reference discharge process,  $Q_r$  is the rated capacity.

In this paper, the working process between every two reference charge and discharge process of the battery is defined as an RW cycle, which reflects the working state of the battery during this period. Feature extraction is performed on the data of each RW cycle to obtain feature vector, as the input of the CNN-BiLSTM. The operational data of each battery are composed of  $N$  RW cycles, the data in each RW cycle includes  $M$  charge and discharge processes  $rw_m$  ( $m = 1, 2, \dots, M$ ). Each charge and discharge process includes  $K$  sampling points. For the  $i$ th ( $i = 1, 2, \dots, N$ ) RW cycle, the constructed feature vector according to the RW cycle is  $x_i$ , of which the  $j$ th feature variable is  $x_{i,j}$ .

The first feature variable  $x_{i,1}$  is the average time of each charge and discharge process  $\bar{t}_i$  in the RW cycle, which can be expressed in Eq. (15):

$$x_{i,1} = \bar{t}_i = \frac{1}{M} \sum_{m=1}^M t(rw_m) \quad (15)$$

where  $t(rw_m)$  is the time of the  $m$ th charge and discharge process. It should be noted that as the battery degrading, the battery needs longer working time to meet the demand, which reflects the battery's working state.

The second feature variable  $x_{i,2}$  is the instantaneous resistance  $\bar{R}_i$  of the battery during discharge process. Since the internal resistance of the battery will increase during working operation, the instantaneous resistance can reflect the battery state, as shown in Eq. (16):

$$x_{i,2} = \bar{R}_i = \frac{1}{M} \sum_{m=1}^M \sum_{k=1}^{K-1} \frac{u_{k+1}(rw_m) - u_k(rw_m)}{i_{k+1}(rw_m) - i_k(rw_m)} \quad (16)$$

where  $u_k$  and  $i_k$  represent the voltage and current at the time of the  $k$ th sampling point, respectively.

In the working process, the charge and discharge capacity of the battery in each cycle can measure the present capacity of the battery. In this sense, the third feature variable  $x_{i,3}$  is the average charge capacity of the battery during each charge process of a single RW cycle shown in Eq. (17):

$$x_{i,3} = \bar{Q}_{ci} = \frac{1}{M} \sum_{m=1}^M \int_0^{t_c} i_c(rw_m, \tau) d\tau \quad (17)$$

where  $i_c$  is the current during the charge process,  $t_c$  is the time of the corresponding charge process.

The fourth feature variable  $x_{i,4}$  is the average discharge capacity of the battery during each discharge process of a single RW cycle shown in Eq. (18):

$$x_{i,4} = \overline{Q_{di}} = \frac{1}{M} \sum_{m=1}^M \int_0^{t_d} i_d(rw_m, \tau) d\tau \quad (18)$$

where  $i_d$  is the current during the discharge process,  $t_d$  is the time of the corresponding discharge process.

In summary, through the feature extraction of the raw measurement data of the battery under random dynamic load conditions, the data under each RW cycle can be finally converted into a 4-dimensional feature vector, which are applied as the input to the neural network.

### 3.3. SOC estimation evaluation indicators

In this paper, root mean square error (RMSE), mean absolute error (MAE) and maximum error (MAX) are applied as the evaluation indicators for SOC estimation performance, as shown in Eqs. (19-21):

$$RMSE = \sqrt{\frac{1}{N} \sum_{i=1}^N (SOC_{pi} - SOC_{ti})^2} \quad (19)$$

$$MAE = \frac{1}{N} \sum_{i=1}^N |SOC_{pi} - SOC_{ti}| \quad (20)$$

$$MAX = \max |SOC_{pi} - SOC_{ti}| \quad (21)$$

where  $N$  denotes the total number of samples in the testing set,  $i$  is the index of the samples.  $SOC_{pi}$  and  $SOC_{ti}$  are the SOC estimated value and SOC ground truth of the  $i$ th testing sample, respectively. Among them, RMSE signifies the robustness of the estimation, MAE represents the accuracy of the estimation and MAX can display the maximum estimation error [16].

### 3.4. CNN-BiLSTM estimation results

The CNN-BiLSTM network is developed to train the algorithm model for each condition, respectively. Since each condition contains the working data of 4 batteries, leave-one-out cross validation is adopted for model training and estimation. In other words, each battery data is employed as the test dataset in turn, and the other 3 battery datasets are employed as the training datasets [26].

Regarding the training process of the CNN-BiLSTM, the conversion of the 4-dimensional features into  $2 \times 2$  matrix is used as the input. The SOC calculated by

working condition: experiment.

↓  
AVG 1,2,7,8 ← leave-one-out cross validation

↑ RMSE 评估.

The number of CNN layers.  
The number of BiLSTM layers.  
The number of BiLSTM neurons.

Preprint submitted to Measurement Science and Technology

11

to入  
CNN-  
BiLSTM  
网络参数  
调整实验

reference charge and discharge cycle after the corresponding RW cycle is used as the label. The convolution kernel in CNN slides on the two-dimensional matrix to realize the spatial feature extraction of the data. Furthermore, the temporal feature of the data is learned through the BiLSTM. Finally, the target SOC is acquired through the fully connected layer.

The CNN part in the neural network mainly includes three convolutional layers and one pooling layers. The number of convolution kernels is 16, 32 and 64, respectively. Moreover, the maxpooling is selected in the pooling layers. The BatchNorm layer is introduced into the CNN-BiLSTM network structure so that the output distribution of the layer is converted into a Gaussian distribution, the advantages of which are to increase the speed of model training and avoid the disappearance and explosion of gradients [27, 28]. The LSTM part in the neural network consists of three hidden layers, each of which has 100, 100 and 200 units, respectively. The CNN-BiLSTM network parameter setting can be shown in Table 2. Correspondingly, Table 3 lists hyperparameter configuration of the proposed model.

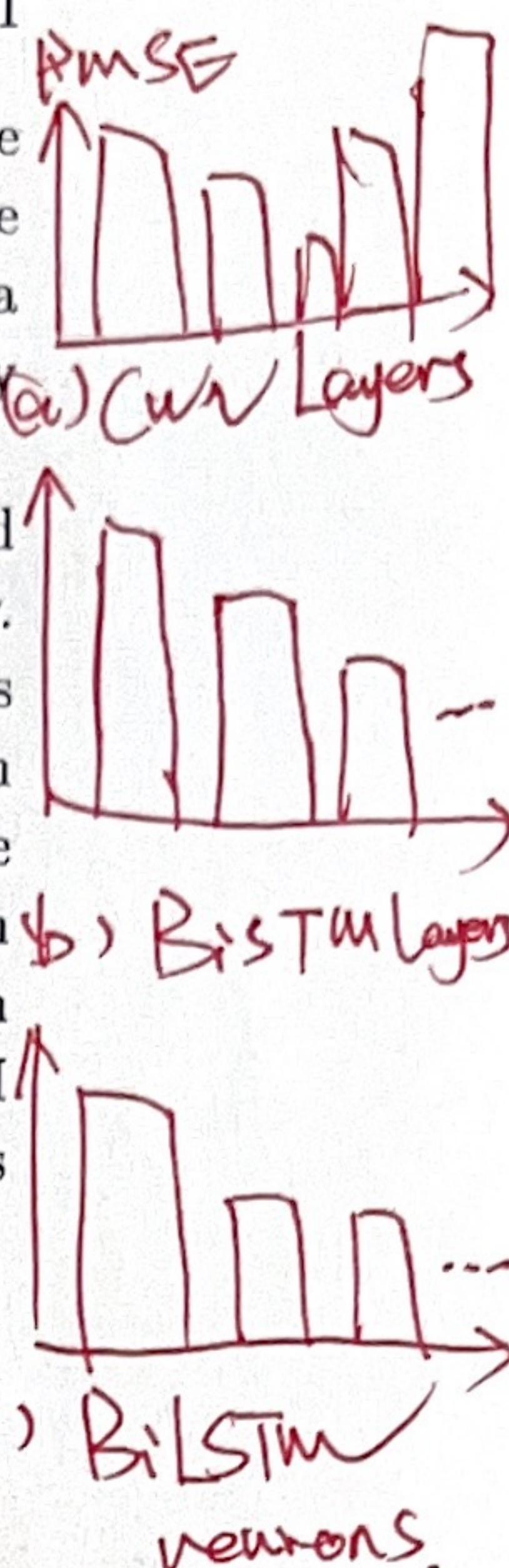


Table 2. The specific parameters settings of CNN-BiLSTM

| Part   | Layer              | Configuration                                 |
|--------|--------------------|---|
| CNN    | Convolution        | filters = 16, kernel size = (2,2), stride = 1 |
|        | Convolution        | filters = 32, kernel size = (2,2), stride = 1 |
|        | BatchNormalization | -   |
| BiLSTM | Convolution        | filters = 64, kernel size = (2,2), stride = 1 |
|        | Max-pooling        | pool size = (2,1), stride = 1                 |
|        | BiLSTM units       | units = 100                                   |
| FC     | BiLSTM units       | units = 100                                   |
|        | BiLSTM units       | units = 200                                   |
|        | Fully connected    | neuron = 1                                    |

↓ > ②) > ③) > ④)

①) CNN - BiLSTM

Table 3. Hyperparameter configuration of CNN-BiLSTM

| Epoch | Learning rate | Loss function | Optimizer |
|-------|---------------|---------------|-----------|
| 1000  | 0.01          | RMSE          | Adam      |

The CNN-BiLSTM network is trained for the battery data under the five operating conditions of 1, 2, 3, 6, 7, respectively. Leave-one-out cross validation is employed to verify the performance of the SOC estimation approach. Table 4 lists the three estimation evaluation indicators of CNN-BiLSTM network for 20 batteries under five conditions.



**Table 4.** CNN-BiLSTM estimation indicators

| Condition | Battery | RMSE   | MAE    | MAX    |
|-----------|---------|--------|--------|--------|
| 1         | RW1     | 0.0189 | 0.0143 | 0.0503 |
|           | RW2     | 0.0125 | 0.0101 | 0.0282 |
|           | RW7     | 0.0177 | 0.0146 | 0.0398 |
|           | RW8     | 0.0201 | 0.0146 | 0.0585 |
| 2         | Overall | 0.0173 | 0.0134 | 0.0442 |
|           | RW3     | 0.0207 | 0.0164 | 0.0445 |
|           | RW4     | 0.0233 | 0.0178 | 0.0583 |
|           | RW5     | 0.0347 | 0.0171 | 0.1465 |
|           | RW6     | 0.0268 | 0.0207 | 0.0532 |
| 3         | Overall | 0.0264 | 0.0180 | 0.0756 |
|           | RW9     | 0.0219 | 0.0164 | 0.0611 |
|           | RW10    | 0.0164 | 0.0141 | 0.0331 |
|           | RW11    | 0.0331 | 0.0245 | 0.1219 |
|           | RW12    | 0.0296 | 0.0237 | 0.0687 |
| 6         | Overall | 0.0253 | 0.0197 | 0.0712 |
|           | RW21    | 0.0099 | 0.0078 | 0.0213 |
|           | RW22    | 0.0315 | 0.0202 | 0.0754 |
|           | RW23    | 0.0080 | 0.0069 | 0.0138 |
|           | RW24    | 0.0123 | 0.0101 | 0.0199 |
| 7         | Overall | 0.0154 | 0.0113 | 0.0326 |
|           | RW25    | 0.0111 | 0.0095 | 0.0195 |
|           | RW26    | 0.0212 | 0.0169 | 0.0365 |
|           | RW27    | 0.0234 | 0.0216 | 0.0331 |
|           | RW28    | 0.0123 | 0.0104 | 0.0206 |
|           | Overall | 0.0170 | 0.0146 | 0.0274 |

### 3.5. CNN-BiLSTM-TF estimation results

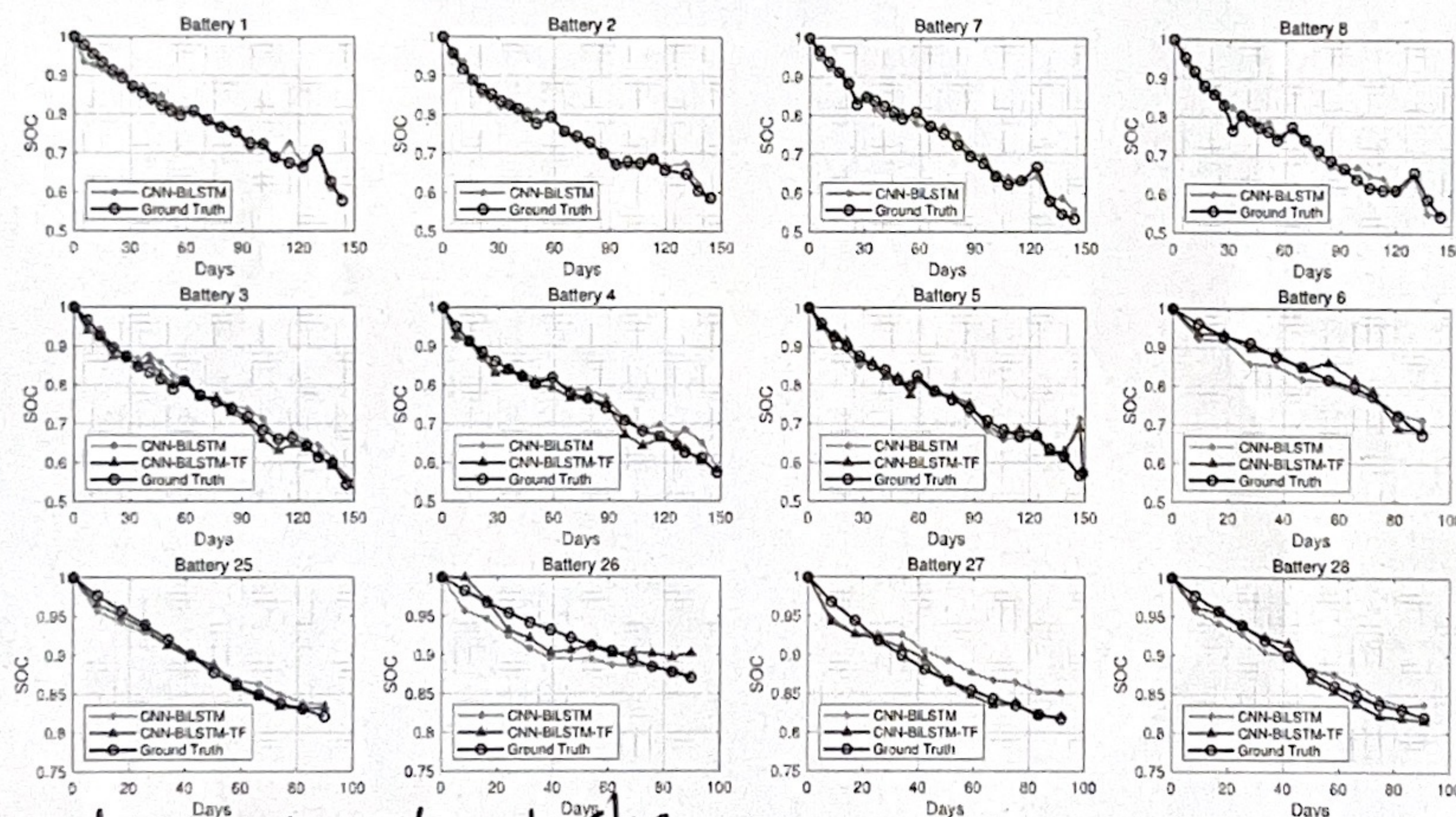
Transfer learning can transfer knowledge and experience from the source domain to the target domain, which can invisibly expand the training data. Furthermore, the robustness and generalization ability of the model can be enhanced, and the training speed can be improved [29, 30]. In this paper, optimization method, the model-based transfer learning, is firstly proposed for SOC estimation.

According to the description in Table 1, the working condition 1 is more representative and applicable to the actual situation, which corresponds to industrial practice. Therefore, the battery data in the condition 1 are considered as the source domain, and the battery data in the conditions numbered 2, 3, 6, 7 are considered as the target domain, so as to achieve model-based transfer learning.

There are four batteries in each operating condition so that four CNN-BiLSTM

**Table 5.** CNN-BiLSTM-TF estimation indicators

| Condition | Battery | RMSE   | MAE    | MAX    |
|-----------|---------|--------|--------|--------|
| 2         | RW3     | 0.0157 | 0.0125 | 0.0300 |
|           | RW4     | 0.0170 | 0.0119 | 0.0382 |
|           | RW5     | 0.0285 | 0.0152 | 0.1200 |
|           | RW6     | 0.0207 | 0.0207 | 0.0382 |
|           | Overall | 0.0205 | 0.0151 | 0.0566 |
| 3         | RW9     | 0.0202 | 0.0146 | 0.0639 |
|           | RW10    | 0.0153 | 0.0125 | 0.0312 |
|           | RW11    | 0.0326 | 0.0261 | 0.0876 |
|           | RW12    | 0.0260 | 0.0202 | 0.0661 |
|           | Overall | 0.0235 | 0.0184 | 0.0622 |
| 6         | RW21    | 0.0075 | 0.0055 | 0.0183 |
|           | RW22    | 0.0258 | 0.0215 | 0.0433 |
|           | RW23    | 0.0075 | 0.0060 | 0.0174 |
|           | RW24    | 0.0086 | 0.0078 | 0.0140 |
|           | Overall | 0.0124 | 0.0102 | 0.0233 |
| 7         | RW25    | 0.0064 | 0.0050 | 0.0113 |
|           | RW26    | 0.0177 | 0.0145 | 0.0316 |
|           | RW27    | 0.0107 | 0.0075 | 0.0256 |
|           | RW28    | 0.0094 | 0.0079 | 0.0152 |
|           | Overall | 0.0111 | 0.0087 | 0.0209 |



More cross-domain transfer tasks:

Figure 5. Estimation results of the proposed approach

$1 \rightarrow 2, 3, 6$   
 $3 \rightarrow 1, 2, 6, 7$   
 $7 \dots$   
 $2 \rightarrow 1, 3, 6, 7$

每个工况有4个电池  $\Rightarrow$  leave-one-out cross validation

Tab : source domain: a  
target domain: b

表格设计

| Condition | RMSE                                    |               | MAE                                |                                    | MAX                                |                                    |
|-----------|---|---------------|------------------------------------|------------------------------------|------------------------------------|------------------------------------|
|           | CNN-BiLSTM                              | CNN-BiLSTM-FF | CNN-BiLSTM                         | (CNN-BiLSTM-TF)                    | CNN-<br>BiLSTM                     | CNN-<br>BiLSTM-TF                  |
| 1         | $T_{21}$<br>$T_{31}$<br>$T_{61} T_{71}$ |               |                                    | $T_{21} T_{31}$<br>$T_{61} T_{71}$ |                                    | $T_{21} T_{31}$<br>$T_{61} T_{71}$ |
| 2         | $T_{12} T_{32}$<br>$T_{62} T_{72}$      |               | $T_{12} T_{32}$<br>$T_{62} T_{72}$ | 14                                 | $T_{12} T_{32}$<br>$T_{62} T_{72}$ | $T_{12} T_{32}$<br>$T_{62} T_{72}$ |

Preprint submitted to Measurement Science and Technology

models can be obtained through leave-one-out cross validation. Therefore, the four models are transferred separately and the model with the best estimation performance is saved. The implementation of the training is to keep the parameters of the spatial feature learning part CNN unchanged. Meanwhile, the parameters of the temporal feature learning part BiLSTM are trained for the target domain. In this sense, the battery data under conditions numbered 2, 3, 6, and 7 are employed for leave-one-out cross validation to evaluate the model estimation performance. Table 5 lists the three estimation evaluation indicators of CNN-BiLSTM-TF network for 16 batteries under four conditions.

This paper uses 12 batteries under working conditions 1, 2, and 7 as examples to visualize the SOC estimation results in Figure 5. The four subgraphs in the first row represent the CNN-BiLSTM estimated results and SOC ground truth for condition 1, and the other subgraphs represent the CNN-BiLSTM network and the CNN-BiLSTM-TF network estimated results and the SOC ground truth for condition 2 and 7.

### 3.6. Discussion

Combining Table 4 and Table 5, the estimation performance is measured by the average of the estimation indicators of the four models under each working condition. The SOC estimation performance of the CNN-BiLSTM and the CNN-BiLSTM-TF is compared in Table 6. Through the compared results in Table 6, the SOC estimation performance of CNN-BiLSTM-TF is better than CNN-BiLSTM network. In this sense, the robustness and accuracy of the model can be improved by transfer learning, and the maximum error of the estimation can be decreased. The reason is that transfer learning can migrate the knowledge and experience learned by the CNN-BiLSTM network in the source domain to the target domain, which expands the training sample data invisibly. Furthermore, the retraining of the network can be avoided, thereby achieving the improvement of the SOC estimation performance.

Compared with the existing literature, this paper has carried out experiments to verify the proposed approach on all available batteries in the dataset, which reflects the applicability of the CNN-BiLSTM-TF network. To express the superiority of the approach, Table 7 represents the results of other data-driven based estimation approaches in some published works and the proposed approach in this paper for the four batteries numbered 9-12 under working condition 3. Furthermore, Table 8 represents the comparison of approaches in other working conditions. Through the compared results in Table 6, Table 7 and Table 8, the proposed CNN-BiLSTM-TF network is able to effectively estimate the SOC of battery under random dynamic load conditions, which is better than some published works.

Condition 1  
source domain

Condition 3  
target domain

**Table 6.** Comparison of CNN-BiLSTM and CNN-BiLSTM-TF

| Condition | RMSE       |               | MAE        |               | MAX        |               |
|-----------|------------|---------------|------------|---------------|------------|---------------|
|           | CNN-BiLSTM | CNN-BiLSTM-TF | CNN-BiLSTM | CNN-BiLSTM-TF | CNN-BiLSTM | CNN-BiLSTM-TF |
| 1         | 0.0173     | -             | 0.0134     | -             | 0.0422     | -             |
| 2         | 0.0264     | <b>0.0205</b> | 0.0180     | <b>0.0151</b> | 0.0756     | <b>0.0566</b> |
| 3         | 0.0253     | <b>0.0235</b> | 0.0197     | <b>0.0184</b> | 0.0712     | <b>0.0622</b> |
| 6         | 0.0154     | <b>0.0124</b> | 0.0113     | <b>0.0102</b> | 0.0326     | <b>0.0233</b> |
| 7         | 0.0170     | <b>0.0111</b> | 0.0146     | <b>0.0087</b> | 0.0274     | <b>0.0209</b> |

**Table 7.** Comparison of results for condition 3 in some published works

| Approach                 | RMSE   |        |        |        |               | MAE    |        |        |        |               | MAX    |        |        |        |               |
|--------------------------|--------|--------|--------|--------|---------------|--------|--------|--------|--------|---------------|--------|--------|--------|--------|---------------|
|                          | RW9    | RW10   | RW11   | RW12   | Overall       | RW9    | RW10   | RW11   | RW12   | Overall       | RW9    | RW10   | RW11   | RW12   | Overall       |
| MFPa[31]                 | 0.0417 | 0.0816 | 0.1208 | 0.0661 | 0.0776        | 0.0339 | 0.0672 | 0.0913 | 0.0549 | 0.0618        | 0.1214 | 0.1631 | 0.4925 | 0.1024 | 0.2199        |
| MFPb[31]                 | 0.0303 | 0.0614 | 0.1163 | 0.1392 | 0.0868        | 0.0241 | 0.0487 | 0.0975 | 0.1269 | 0.0743        | 0.0641 | 0.0962 | 0.4188 | 0.2045 | 0.1959        |
| MFPc[31]                 | 0.0183 | 0.0352 | 0.0907 | 0.1383 | 0.0706        | 0.0147 | 0.0222 | 0.0795 | 0.1281 | 0.0611        | 0.3520 | 0.7380 | 0.3671 | 0.1515 | 0.4022        |
| D-LSTM-RN short-term[31] | 0.0225 | 0.0264 | 0.0625 | 0.0257 | 0.0343        | 0.0172 | 0.0202 | 0.0408 | 0.0181 | 0.0241        | 0.0456 | 0.0616 | 0.3601 | 0.0717 | 0.1348        |
| D-LSTM-RN long-term[31]  | 0.0603 | 0.0797 | 0.1303 | 0.2052 | 0.1189        | 0.0477 | 0.0612 | 0.1087 | 0.1884 | 0.1015        | 0.1170 | 0.1636 | 0.2704 | 0.2214 | 0.1931        |
| EKF[32]                  | 0.0617 | 0.0339 | 0.0331 | 0.0597 | 0.0471        | 0.0579 | 0.0291 | 0.0289 | 0.0547 | 0.0427        | 0.0901 | 0.0632 | 0.0588 | 0.0894 | 0.0754        |
| DBN-KF[32]               | 0.0226 | 0.0264 | 0.0263 | 0.0193 | 0.0237        | 0.0181 | 0.0212 | 0.0190 | 0.0154 | 0.0184        | 0.0679 | 0.0693 | 0.0856 | 0.0891 | 0.0780        |
| CNN-BiLSTM-TF            | 0.0202 | 0.0153 | 0.0326 | 0.0260 | <b>0.0235</b> | 0.0146 | 0.0125 | 0.0261 | 0.0202 | <b>0.0184</b> | 0.0639 | 0.0312 | 0.0876 | 0.0661 | <b>0.0622</b> |

**Table 8.** Comparison of results for several conditions

| Condition | RMSE   |               |             |               | MAE    |               |             |               |
|-----------|--------|---------------|-------------|---------------|--------|---------------|-------------|---------------|
|           | GP[25] | CNN-BiLSTM-TF | Deep GP[33] | CNN-BiLSTM-TF | GP[25] | CNN-BiLSTM-TF | Deep GP[33] | CNN-BiLSTM-TF |
| 2         | 0.1160 | <b>0.0205</b> | -           | -             | -      | 0.0151        | -           | -             |
| 3         | 0.1860 | <b>0.0235</b> | -           | -             | -      | 0.0184        | -           | -             |
| 6         | 0.1250 | <b>0.0154</b> | -           | 0.040         | -      | <b>0.0102</b> | -           | -             |
| 7         | -      | 0.0170        | -           | -             | -      | 0.0087        | -           | -             |

#### 4. Conclusion

To integrate the spatial and temporal characteristics of the data, this paper proposes a deep learning approach to estimate SOC of the battery under random dynamic load conditions. The data are obtained from the working process as the features. The battery dataset under one working condition is used as source domain to establish CNN-BiLSTM network. Afterwards, the battery dataset under other working conditions are used as target domain. The trained CNN-BiLSTM network under the source domain is transferred to the target domain through transfer learning. Finally, the CNN-BiLSTM-TF network can be applied for online SOC estimation, the estimation performance of which is evaluated by the corresponding indicators. The main contributions of the SOC estimation approach can be described as: (1) It is proposed to estimate SOC with the aid of CNN, from which the spatial feature can be learnt. (2) Towards to extract temporal feature of data, it is proposed to estimate SOC through BiLSTM. (3) Transfer learning is proposed to estimate SOC for the first time, which improves the estimation performance. (4) The SOC estimation approach proposed in this paper is verified by the battery dataset under random dynamic load condition provided by the NASA Ames

this paper adopts a model-based transfer learning method to transfer the deep learning model from the source domain to target domain, thereby promoting the SOC estimation performance.

Research Center and the performance based on CNN-BiLSTM-TF network is better than some published works.

~~Do I have any notes?~~ *Limitation, the distribution difference between the source domain data and the target domain*

## References

- [1] V. Pop, H. J. Bergveld, P. Notten, and P. P. Regtien, "State-of-the-art of battery state-of-charge determination," *Measurement science and technology*, vol. 16, no. 12, p. R93, 2005.
- [2] Á. Porras-Hermoso, S. Pindado, and J. Cubas, "Lithium-ion battery performance modeling based on the energy discharge level," *Measurement Science and Technology*, vol. 29, no. 11, p. 117002, 2018.
- [3] Y. Wu, M. Yang, Y. Wang, H. Li, Z. Gui, and J. Liu, "Pole-piece position distance identification of cylindrical lithium-ion battery through x-ray testing technology," *Measurement Science and Technology*, vol. 32, no. 4, p. 045405, 2021.
- [4] G. Chen, Z. Liu, H. Su, and W. Zhuang, "Electrochemical-distributed thermal coupled model-based state of charge estimation for cylindrical lithium-ion batteries," *Control Engineering Practice*, vol. 109, p. 104734, 2021.
- [5] C. Chang, Y. Zheng, W. Sun, and Z. Ma, "Lpv estimation of soc based on electricity conversion and hysteresis characteristic," *Journal of Energy Engineering*, vol. 145, no. 6, p. 04019026, 2019.
- [6] J. Hong, Z. Wang, W. Chen, L.-Y. Wang, and C. Qu, "Online joint-prediction of multi-forward-step battery soc using lstm neural networks and multiple linear regression for real-world electric vehicles," *Journal of Energy Storage*, vol. 30, p. 101459, 2020.
- [7] M.-K. Tran, A. Meuwala, S. Panchal, K. Raahemifar, M. Fowler, and R. Fraser, "Effect of integrating the hysteresis component to the equivalent circuit model of lithium-ion battery for dynamic and non-dynamic applications," *Journal of Energy Storage*, vol. 32, p. 101785, 2020.
- [8] W. Li, D. Cao, D. Jöst, F. Ringbeck, M. Kuipers, F. Frie, and D. U. Sauer, "Parameter sensitivity analysis of electrochemical model-based battery management systems for lithium-ion batteries," *Applied Energy*, vol. 269, p. 115104, 2020.
- [9] M. Zeng, P. Zhang, Y. Yang, C. Xie, and Y. Shi, "Soc and soh joint estimation of the power batteries based on fuzzy unscented kalman filtering algorithm," *Energies*, vol. 12, no. 16, p. 3122, 2019.
- [10] R. Xiong, Y. Zhang, H. He, X. Zhou, and M. G. Pecht, "A double-scale, particle-filtering, energy state prediction algorithm for lithium-ion batteries," *IEEE Transactions on Industrial Electronics*, vol. 65, no. 2, pp. 1526–1538, 2017.
- [11] H. Zhu, Y. Liu, and C. Zhao, "Parameter identification and soc estimation of lithium ion battery," *Journal of Hunan University*, vol. 41, no. 3, pp. 37–42, 2014.
- [12] M. H. Lipu, M. Hannan, A. Hussain, A. Ayob, M. H. Saad, T. F. Karim, and D. N. How, "Data driven state of charge estimation of lithium-ion batteries: Algorithms, implementation factors, limitations and future trends," *Journal of Cleaner Production*, p. 124110, 2020.
- [13] Z. Deng, X. Hu, X. Lin, Y. Che, L. Xu, and W. Guo, "Data-driven state of charge estimation for lithium-ion battery packs based on gaussian process regression," *Energy*, vol. 205, p. 118000, 2020.
- [14] C. Hu, G. Jain, C. Schmidt, C. Strief, and M. Sullivan, "Online estimation of lithium-ion battery capacity using sparse bayesian learning," *Journal of Power Sources*, vol. 289, pp. 105–113, 2015.
- [15] S. Shen, M. Sadoughi, X. Chen, M. Hong, and C. Hu, "A deep learning method for online capacity estimation of lithium-ion batteries," *Journal of Energy Storage*, vol. 25, p. 100817, 2019.
- [16] P. Venugopal *et al.*, "State-of-health estimation of li-ion batteries in electric vehicle using indrnn under variable load condition," *Energies*, vol. 12, no. 22, p. 4338, 2019.
- [17] M. Duan, K. Li, C. Yang, and K. Li, "A hybrid deep learning cnn-elm for age and gender classification," *Neurocomputing*, vol. 275, pp. 448–461, 2018.
- [18] R. R. Richardson, C. R. Birk, M. A. Osborne, and D. A. Howey, "Gaussian process regression for in

- situ capacity estimation of lithium-ion batteries," *IEEE Transactions on Industrial Informatics*, vol. 15, no. 1, pp. 127–138, 2018.
- [19] J. Zhang, Y. Jiang, H. Luo, and S. Yin, "Prediction of material removal rate in chemical mechanical polishing via residual convolutional neural network," *Control Engineering Practice*, vol. 107, p. 104673, 2021.
  - [20] J. Gu, Z. Wang, J. Kuen, L. Ma, A. Shahroudy, B. Shuai, T. Liu, X. Wang, G. Wang, J. Cai *et al.*, "Recent advances in convolutional neural networks," *Pattern Recognition*, vol. 77, pp. 354–377, 2018.
  - [21] F. Xu, Z. Li, Z. Nie, H. Shao, and D. Guo, "New recurrent neural network for online solution of time-dependent underdetermined linear system with bound constraint," *IEEE Transactions on Industrial Informatics*, vol. 15, no. 4, pp. 2167–2176, 2018.
  - [22] S. Si, D. Tao, and B. Geng, "Bregman divergence-based regularization for transfer subspace learning," *IEEE Transactions on Knowledge and Data Engineering*, vol. 22, no. 7, pp. 929–942, 2010.
  - [23] K. Weiss, T. M. Khoshgoftaar, and D. D. Wang, "A survey of transfer learning," *Journal of Big Data*, vol. 3, no. 1, p. 9, 2016.
  - [24] B. Bole, C. S. Kulkarni, and M. Daigle, "Adaptation of an electrochemistry-based li-ion battery model to account for deterioration observed under randomized use," *Conference of the Prognostics and Health Management Society*, 2014.
  - [25] R. R. Richardson, M. A. Osborne, and D. A. Howey, "Battery health prediction under generalized conditions using a gaussian process transition model," *Journal of Energy Storage*, vol. 23, pp. 320–328, 2019.
  - [26] D. R. Roberts, V. Bahn, S. Ciuti, M. S. Boyce, J. Elith, G. Guillera-Arroita, S. Hauenstein, J. J. Lahoz-Monfort, B. Schröder, W. Thuiller *et al.*, "Cross-validation strategies for data with temporal, spatial, hierarchical, or phylogenetic structure," *Ecography*, vol. 40, no. 8, pp. 913–929, 2017.
  - [27] I. Schiopu and A. Munteanu, "Residual-error prediction based on deep learning for lossless image compression," *Electronics Letters*, vol. 54, no. 17, pp. 1032–1034, 2018.
  - [28] S. Ioffe and C. Szegedy, "Batch normalization: Accelerating deep network training by reducing internal covariate shift," *arXiv preprint arXiv:1502.03167*, 2015.
  - [29] C. Sun, M. Ma, Z. Zhao, S. Tian, R. Yan, and X. Chen, "Deep transfer learning based on sparse autoencoder for remaining useful life prediction of tool in manufacturing," *IEEE Transactions on Industrial Informatics*, vol. 15, no. 4, pp. 2416–2425, 2018.
  - [30] A. S. Qureshi, A. Khan, A. Zameer, and A. Usman, "Wind power prediction using deep neural network based meta regression and transfer learning," *Applied Soft Computing*, vol. 58, pp. 742–755, 2017.
  - [31] C. B. Salucci, A. Bakdi, I. K. Glad, E. Vanem, and R. De Bin, "Simple statistical models and sequential deep learning for lithium-ion batteries degradation under dynamic conditions: Fractional polynomials vs neural networks," *arXiv preprint arXiv:2102.08111*, 2021.
  - [32] D. Liu, L. Li, Y. Song, L. Wu, and Y. Peng, "Hybrid state of charge estimation for lithium-ion battery under dynamic operating conditions," *International Journal of Electrical Power and Energy Systems*, vol. 110, pp. 48–61, 2019.
  - [33] P. Tagade, K. S. Hariharan, S. Ramachandran, A. Khandelwal, A. Naha, S. M. Kolake, and S. H. Han, "Deep gaussian process regression for lithium-ion battery health prognosis and degradation mode diagnosis," *Journal of Power Sources*, vol. 445, p. 227281, 2020.